



A comparison of six photometric redshift methods applied to 1.5 million luminous red galaxies

F. B. Abdalla,¹★ M. Banerji,²★ O. Lahav¹★ and V. Rashkov³

¹Department of Physics and Astronomy, University College London, Gower Street, London WC1E 6BT

²Institute of Astronomy, University of Cambridge, Madingley Road, Cambridge CB3 0HA

³UC Santa Cruz, 1156 High Street, Santa Cruz, CA 95064, USA

Accepted 2011 July 4. Received 2011 March 4

ABSTRACT

We present an updated version of MegaZ-LRG (Collister et al. 2007) with photometric redshifts derived with the neural network method ANNz as well as five other publicly available photometric redshift codes (HyperZ, SDSS, Le PHARE, BPZ and ZEBRA) for ~ 1.5 million luminous red galaxies (LRGs) in SDSS DR6. This allows us to identify how reliable codes are relative to each other if used as described in their public release. We compare and contrast the relative merits of each code as well as the different templates using $\sim 13\,000$ spectroscopic redshifts from the 2SLAQ sample, and note that this comparison is only valid for LRGs. We find that the performance of each code depends on the figure of merit used to assess it, and note that all codes suffer from a redshift-dependent bias. As expected, the availability of a complete training set means that the training method performs best in the intermediate redshift bins where there are plenty of training objects. Codes such as Le PHARE, which use new observed templates, perform best in the lower redshift bins. All codes produce reasonable photometric redshifts, the 1σ scatters ranging from 0.057 to 0.097 if averaged over the entire redshift range. We also perform tests to check whether a training set from a small region of the sky such as 2SLAQ produces biases if used to train over a larger area of the sky. We conclude that this is not likely to be a problem for future wide-field surveys. The complete photometric redshift catalogue including redshift estimates and errors on these from all the six methods as well as the configuration files used to run the various codes can be found at www.ast.cam.ac.uk/~mbanerji/Research/MegaZRGDR6/megaz.html.

Key words: methods: data analysis – galaxies: distances and redshifts.

1 INTRODUCTION

Photometric redshifts ($photo-z$) will be one of the key ingredients for us to improve our understanding of the Universe in the next 1 decade or so. To date, galaxy large-scale structure surveys relied mainly on spectroscopic redshifts ($spec-z$) to produce high-precision power spectrum measurements of the galaxy distribution (e.g. Cole et al. 2005; Percival et al. 2007). Combined with cosmic microwave background (CMB) experiments, these surveys have provided evidence that the Universe is flat and is likely to be dominated by a dark energy component (Komatsu et al. 2009).

However, a considerable step-up in the size of the spectroscopic surveys will be a hard task to perform for technical reasons. Several multifibre optical spectrographs are currently being built (FMOS) (Dalton et al. 2006) or being designed (WFMOS), but it is unlikely

that they will be able to survey a considerable part of the sky. On the other hand, radio interferometers may be able to perform spectroscopic surveys of the sky reasonably quickly (Blake et al. 2004; Abdalla & Rawlings 2005) but the time-scale for the technical advances to allow for this will be relatively long.

The alternative to a full spectroscopic survey is to obtain multicolour images of the sky and perform photometric redshift estimates for the galaxies that are available (e.g. Bolzonella, Miralles & Pelló 2000; Loh & Spillar 1986; Connolly et al. 1995; Koo 1999; Benítez 2000; Bolzonella, Miralles & Pelló 2000; Budavári et al. 2001; Wolf et al. 2001; Arnouts et al. 2002; Csabai et al. 2003; Firth, Lahav & Somerville 2003; Babbedge et al. 2004; Collister & Lahav 2004; Feldmann et al. 2006; Ilbert et al. 2006; Hildebrandt, Wolf & Benítez 2008; Rowan-Robinson et al. 2008). In a pilot study with high-redshift luminous red galaxies (LRGs) it has been shown (Padmanabhan et al. 2005; Blake et al. 2007) that producing large-scale measurements with photometric redshifts is possible and competitive with a smaller spectroscopic redshift survey. Using the same data set, Blake, Collister & Lahav (2008) have shown that

*E-mail: fba@star.ucl.ac.uk (FBA); mbanerji@ast.cam.ac.uk (MB); lahav@star.ucl.ac.uk (OL)

photometric redshifts can also be used to study small-scale halo model signatures.

On the other hand, there are many caveats of photometric redshifts that have to be assessed in order for us to be completely confident that these measurements are reliable to the level of systematics that we expect in future surveys. For instance, Blake et al. (2007) have performed a detailed study of whether star-galaxy separation influences the cosmological measurements given that the LRGs that have been selected are contaminated at the per cent level by M-type stars which have similar colours. They have also assessed whether there is a significant contamination from dust corrections in the galaxy, by obtaining estimates of the power spectrum in different regions of obscuration in the sky. They find that the stellar contamination and the dust variations affect the cosmological measurements but not significantly given their statistical error bars.

We extend this analysis concentrating on the level of systematic effects that is introduced by the use of different photometric redshift techniques. We have selected the same sample as was selected in the MegaZ-LRG catalogue (Collister et al. 2007) and used several different photometric redshift techniques on the same galaxies available from the literature, including artificial neural networks, template-fitting techniques and Bayesian techniques. We note here that LRGs have a well-defined 4000-Å break, hence this strong feature makes photometric redshift estimation an easier task. Here all codes compared produce good-quality photometric redshifts and we are comparing more subtle differences between codes. The full cosmological analysis of this data set is published in Thomas et al. (2010, 2011a, 2011b).

In Section 2 we describe the MegaZ-LRG data used. In Section 3 we describe all the methods we have used to estimate the photometric redshifts for the LRG sample. In Section 4 we compare different statistics for the different photo- z results. We perform an analysis to check for gradients across the sky which could arise from training sets if they only belong to a small area of the sky in Section 5 and we present the catalogue in Section 6. Our conclusions are drawn in Section 7.

2 DATA

We use galaxy photometry in a DR6 equivalent to the MegaZ-LRG catalogue, a photometric-redshift catalogue of LRGs based

on the imaging component of the SDSS fourth Data Release. The construction of this catalogue follows the same prescription as in Collister et al. (2007). Here we only outline briefly the description of the catalogue. For details on the construction of this catalogue, see Collister et al. (2007).

2.1 Selection criteria

The MegaZ-LRG catalogue is selected from the SDSS imaging data base using a series of colour and magnitude cuts (Collister et al. 2007) which were designed to match the selection criteria of the 2dF-SDSS LRG and Quasar (2SLAQ) survey (Cannon et al. 2006). 2SLAQ is a spectroscopic follow-up combining the SDSS photometric survey and the spectroscopy from the Two-degree Field (2dF) instrument of the Anglo-Australian Telescope (AAT) (see Fig. 1).

The spectroscopic redshifts available from 2SLAQ were used to train and test the photometric redshift code, which we then applied to the entire set of LRGs selected from the SDSS imaging data base. Around 10 000 objects in selected fields of the SDSS equatorial stripe (at declination $\delta \approx 0^\circ$) were available. The 2SLAQ survey demonstrated that these selection criteria are ≈ 95 per cent efficient in the identification of intermediate-redshift ($0.4 < z < 0.7$) LRGs. The most significant contaminant, accounting for virtually all of the remaining ≈ 5 per cent of objects, is M-type stars.

The 2SLAQ selection criteria fluctuated a little at the beginning of the survey. Specifically, the faint limit of the i -band magnitude i_{dev} (the total magnitude estimated using a deVaucouleurs profile), and the minimum value of d_\perp (a colour variable used to select LRGs), were varied slightly. For the majority of the 2SLAQ survey, the criteria $i_{\text{dev}} \leq 19.8$ and $d_\perp \geq 0.55$ were used. For further details on this, see Cannon et al. (2006).

We note that our training subsample is extrapolated in the sky position, hence it does not spatially cover the entire photometric population. The 2SLAQ targets lie exclusively in the equatorial stripe at declination $\delta \approx 0^\circ$, so it may not fully trace effects such as dust extinction which depend on sky coordinate. One of the important aims of this study is to assess how much this sky extrapolation biases the final photo- z measurements with a training set method. This is important because the resolution of the maps used

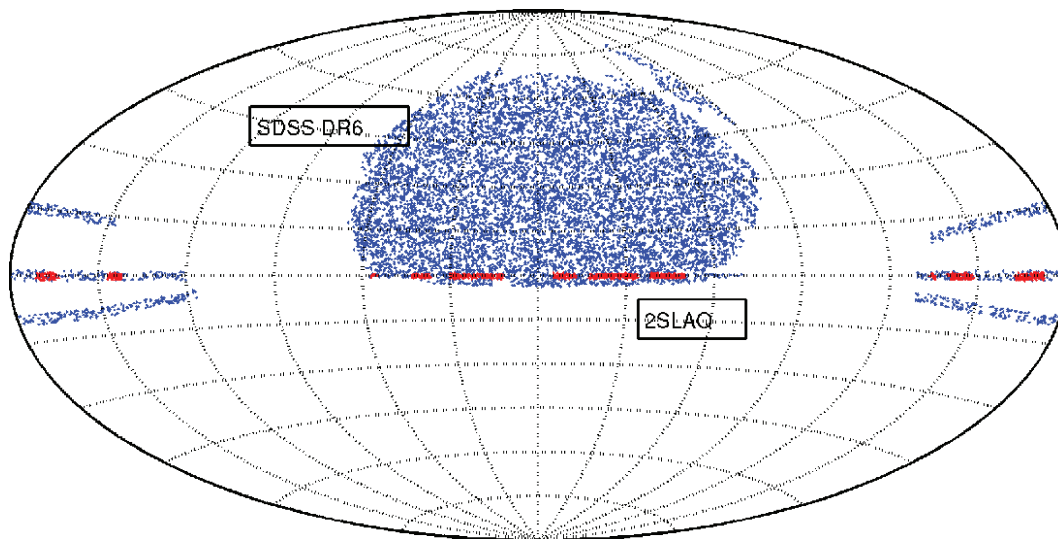


Figure 1. Map of the MegaZ-LRG sample (blue) covering the SDSS DR6 area as well as the 2SLAQ sample (red). For clarity only a random subsample of galaxies has been plotted.

Table 1. Publicly available software packages for photo- z estimation, to date and to our knowledge. In this work we have used six representative codes from this table, namely HyperZ, SDSS, BPZ, ANNz, ZEBRA and Le PHARE.

Code	Authors	Method	Web link
HyperZ	Bolzonella et al.	Template	http://webast.ast.obs-mip.fr/hyperz/
SDSS template	SDSS pipeline	LRG Template	N/A, code obtained from N. Padmanabhan
bpz	Benitez	Template + Bayesian priors	http://acs.pha.jhu.edu/~txitxo/bpzdoc.html
ANNz	Collister & Lahav	Neural Networks	http://zuserver2.star.ucl.ac.uk/~lahav/annz.html
ZEBRA	Feldmann et al.	Template, Bayesian, Hybrid	www.exp-astro.phys.ethz.ch/ZEBRA
Kcorrect	Blanton	Model templates	http://cosmo.nyu.edu/blanton/kcorrect/
Le PHARE	Arnouts & Ilbert	Template	www.oamp.fr/people/arnouts/LE_PHARE.html
EAZY	Brammer et al.	Template	www.astro.yale.edu/eazy/
LRT Libraries	Assef et al.	Template	http://www.astronomy.ohio-state.edu/~rjassem/lrt/

for extinction correction is low. Hence the Schlegel et al. extinction applied to calculate the dereddened galaxy magnitudes may be slightly incorrect.

3 PHOTOMETRIC REDSHIFT ESTIMATORS

This section describes how we obtained the photometric redshifts for galaxies in the 2SLAQ sample. We have subdivided the 9955 galaxies from 2SLAQ into a training sample (4473 galaxies) and a testing sample (5482 galaxies). The training sample was used to train the training part of the codes presented here. The testing sample was chosen such that enough galaxies remained in the training sample. These training set galaxies were randomly chosen.

We have used several different codes from the literature to provide photometric redshift estimates as well as redshift errors for a subset of the 2SLAQ sample. Even for codes that did not require a training set, the test sample of 5482 objects was used to evaluate photometric redshifts so as to compare code outputs on the same galaxies and therefore avoid introducing biases in our study.

We emphasize here that the comparison we are undertaking is a high-level comparison, i.e. we are comparing end products without decomposing the problem into smaller parts in order to potentially assess where discrepancies are arising, in other words comparing codes as black boxes. Therefore it is a comparison of the ensemble of codes plus galaxy libraries used with each code. We argue that this is a valid comparison as this is what a naive user of these publicly available codes would get to do should they choose a code without a proper basis. We also argue that a full analysis is needed to have the highest level of confidence in photometric redshifts and believe that this is being done by the Photometric Accuracy Testing Program (PHAT) collaboration.¹

3.1 Methodology: codes considered in this work

Here we give a brief description of the codes we have used in this work (see Table 1). For a more general description of photo- z methods we refer the reader to Lahav, Abdalla & Banerji (2008) and Budavári (2009).

3.1.1 SDSS template-fitting code

The template-fitting technique in photometric redshift estimation is a χ^2 fit between the data and a given set of templates for those

galaxies. For the purpose of redshift estimation, the galaxy templates usually come from stellar population synthesis models (e.g. Fioc & Rocca-Volmerange 1997; Bruzual & Charlot 2003). A linear combination of templates is used. The coefficients c_i of the templates are the free parameters for the minimization. We note that $\Psi^i(z)$ is the set of templates observed at redshift z and f_α is the observed flux in filter α with an error of σ_α . The photometric redshift is found via χ^2 :

$$\chi^2(c_i, z) = \sum_{\alpha} \left(\frac{f_{\alpha} - R_{\alpha}(\sum_i c_i \Psi^i(z))}{\sigma_{\alpha}} \right)^2, \quad (1)$$

where $R_{\alpha}(\Psi)$ is the flux of spectrum Ψ through filter α .

The greatest disadvantage of this method (which also applies to all the other template-fitting techniques presented here) is the potential mismatch between the templates used for the fitting and the properties of the sample of galaxies for which one wants to estimate the redshifts. A hybrid method can be used, in which in order to calibrate the templates to a better representation of the studied galaxy sample one would use a training set with known spectroscopic redshifts (Ilbert et al. 2006) and similar properties to the galaxies whose redshifts need to be estimated. The SDSS code used here applies a hybrid method to the LRG sample using a modified elliptical galaxy template, adjusted to represent an LRG spectrum after three iterations of correction. Given that early-type galaxies evolve passively, only one template is used in the code.

3.1.2 HyperZ

HyperZ (Bolzonella et al. 2000) was the first publicly available photo- z code and has consequently been widely used in the literature for photometric redshift estimation. It is a simple template-fitting code that can be used in conjunction with two sets of basis spectral energy distributions (SEDs), namely the observed Coleman, Wu & Weedman (1980) templates (CWW hereafter) or the synthetically generated Bruzual & Charlot (2003) templates (BC hereafter). HyperZ takes as its inputs the photometric catalogue of galaxies with magnitudes and errors on magnitudes through the different filters specified in the filter set, as well as a list of spectral templates to be used in the χ^2 minimization. Various different reddening laws can also be implemented in order to account for the effect of interstellar dust on the shape of the SED. The damping of the Ly α forest increasing with redshift is modelled according to Madau (1995). We have experimented with a variety of different basis template sets including the four CWW templates and interpolations between them (15 templates in total) as well as the eight synthetic BC templates.

¹ http://www.astro.caltech.edu/twiki_phat/bin/view/

We find the BC templates to produce considerably better photo-z outputs than the CWW and interpolated CWW template sets. In order to demonstrate the effects of using two different template sets to calculate photometric redshifts with the same code, we present results obtained using both the four CWW templates roughly corresponding to types E, Sbc, Scd and Im, and the eight BC templates roughly corresponding to types Single Burst, E, S0, Sa, Sb, Sc, Sd and Im.

We have also considered the photo-z outputs with no correction for reddening due to dust in the observed galaxy and with a Calzetti reddening law (Calzetti, Kinney & Storchi-Bergmann 1994) applied to the templates for all the template sets considered. In all the cases we find that including an extinction correction for the host galaxy slightly worsens the photometric redshift estimate. This is likely because the observed CWW templates for example already include the effects of this dust extinction in the host galaxy. Our final HyperZ outputs therefore make no additional correction for reddening by dust in the host galaxy.

We used magnitudes in all the five SDSS optical bands even though the photometric uncertainties in the *u*-band are large and therefore would contribute to a larger scatter in the photo-z estimate. We have checked that removing the *u*-band data does in fact worsen the photo-z estimate.

We note here that other template-based methods are also available for photo-z estimation such as ImpZ (Rowan-Robinson, private communication), KCORRECT (Blanton & Roweis 2007), EAZY (Brammer, van Dokkum & Coppi 2008) and the LRT Libraries (Assef et al. 2008). These have not been presented in this comparison.

3.1.3 ANNz

When a representative training set is available, training methods become a viable option to use instead of template-fitting methods. The basic principle of training methods is the derivation of a parametrization of redshift through the magnitudes of the galaxies in a training set. This parametrization is then applied to galaxies for which no spectroscopy is available, yielding an estimate of the photometric redshift. One of the training methods used here comprises artificial neural networks (Collister & Lahav 2004). Neural networks have been used for the estimation of photo-z in data (Collister et al. 2007) as well as forecasts of photometric redshifts for future data (Abdalla et al. 2008; Banerji et al. 2008). An artificial neural network is made up of several layers, each consisting of a number of nodes. The first layer receives the galaxy magnitudes as inputs, while the last layer outputs the estimated photometric redshift. The layers in between could consist of any number of nodes each. The nodes are interconnected so that a node in a given layer is connected to all nodes in the adjacent layers, with every connection carrying a weight w_{ij} , where i and j describe the two nodes. Each node i is assigned a value u_i and an activation function $g_i(u_i)$ is evaluated:

$$g_i(u_i) = \frac{1}{1 + \exp(-u_i)}. \quad (2)$$

The value of a subsequent node j is then calculated as the summation of the weighted values of the activation functions of all nodes i pointing to it:

$$u_j = \sum_i w_{ij} g_i(u_i). \quad (3)$$

When a network is trained, the weights of all node connections are determined by minimizing a cost function E evaluated on the

training set of galaxies where

$$E = \sum_k [z_{\text{phot}}(w, m_k) - z_{\text{spec},k}]^2 \quad (4)$$

and the photometric redshift given the input m_k for galaxy k from the training set is $z_{\text{phot}}(w, m_k)$, and the spectroscopic redshift of the galaxy is $z_{\text{spec},k}$. We use an assortment of four networks, with different initial random seeds so that we can ensure that the algorithm does not converge in a specific local minimum with a high E .

To avoid an overfitting, every network is tested on a validation set of galaxies, whose spectroscopic redshifts are also known. The network with the lowest value of E as calculated on the validation set is selected and the photometric sample is run through it for redshift estimation (Collister & Lahav 2004).

The artificial neural networks used in ANNz can be described as follows: $N_{\text{in}}:N_1:N_2:\dots:N_{\text{out}}$, where N_{in} and N_{out} are respectively the number of input and output parameters, while N_i is the number of nodes in the i th intermediate layer. In the case of photometric redshift estimation using MegaZ-LRG, a network of the form 5:10:10:1 was used, this was found empirically to be optimal (Firth et al. 2003; Collister et al. 2007).

3.1.4 BPZ

An extension of the above HyperZ likelihood (χ^2) approach is to incorporate priors, with the Bayesian framework. Benítez (2000) formulated the problem as follows. The probability of a galaxy with colour C and magnitude m having a redshift z is

$$p(z|C, m) = \frac{p(z|m)p(C|z)}{p(C)} \propto p(z|m)p(C|z), \quad (5)$$

where the term $p(C|z)$ is the conventional redshift likelihood employed e.g. by HyperZ, and $p(C)$ is just a normalization. The new important ingredient is $p(z|m)$, which brings in the prior knowledge of the magnitude redshift distribution. With the aid of the extra information (prior), this approach is effective in avoiding catastrophic errors of placing a galaxy at an unrealistic redshift.

BPZ can function in a Bayesian and maximum likelihood (ML hereafter) module and therefore produces two outputs for the photometric redshift. The ML method simply picks the highest maximum over all the likelihoods that come from different galaxy types as its redshift estimate whereas the Bayesian method averages over all the likelihoods after weighting them by their prior probabilities.

BPZ also takes as its input a photometric catalogue with magnitudes in different filters and their corresponding errors. The BPZ templates include the four CWW templates as well as the spectra of two starbursting galaxies from Kinney et al. (1996). In this study we added nine interpolations between each of the four CWW templates to the BPZ template list to produce a more complete list of basis SEDs. This gives us a set of 38 basis templates for BPZ to use. We find that ~ 17 of these templates concentrated towards the early types are sufficient to produce the best photometric redshift estimate. Adding more templates does not improve the photo-z scatter. We have also used two further points of interpolation between each of the templates in colour space as specified by the INTERP parameter in BPZ. A flat prior was used throughout the calculation resulting in very similar results from the Bayesian and ML runs.

The BPZ output includes two photo-z estimates from the Bayesian and ML runs as well as a quantity called *odds* that is the amount of probability contained between $-0.12(1+z)$ and $0.12(1+z)$ around the Bayesian photo-z estimate. In order to select galaxies that only have a single compact peak in their probability

distribution, we need to consider those galaxies with odds > 0.95 at the very least and odds > 0.99 for a robust estimate (Benítez, private communication). In the first case, we select out 4811 of the 5482 galaxies and in the second case we are left with 3689 of the 5482 galaxies. The Bayesian output from BPZ, with galaxies with odds > 0.99 selected, gives us the best photo-z estimate and it is this result that we use as the BPZ output in the plots.

3.1.5 Le PHARE – PHotometric Analysis for Redshift Estimations

Le PHARE² is very similar to HyperZ in that a set of template SEDs together with a filter set are used to determine a set of model magnitudes used in the photometric redshift calculation. These are then compared to the observed magnitudes using a χ^2 minimization in order to compute the redshift of an object. The Le PHARE package includes various template sets used to construct the library of model magnitudes. These include the Coleman, Wu and Weedman and Kinney starburst templates, an extended CWW template set with 72 interpolations between the standard CWW templates, 42 synthetic GISSEL templates as well as the observed templates of Poggianti. We have experimented with using these various template sets for photo-z estimation on our sample of 5482 2SLAQ objects and found the best photometric redshifts to be obtained with the eight Poggianti templates corresponding to galaxy types Ell, S0, Sa, Sb, Sc, Sd, SB2 and SB1. The 42 GISSEL templates give slightly worse photo-z outputs than the Poggianti templates but the scatter on the photometric redshift when using the extended sample of 72 interpolated CWW templates is ~ 30 per cent worse than that obtained using the eight Poggianti templates. Therefore, we can see that in a template-based method, we do not necessarily gain in redshift accuracy by adding more model SEDs to our library. We note here that it is likely that best results would be obtained if the templates are selected in a similar way to the observed sample to minimize degeneracies.

Le PHARE also includes various prescriptions to correct for extinction by dust in the host galaxy. We have tried running Le PHARE with different extinction laws assuming $E(B - V) = 0.034$ and find that in all the cases, the photo-z estimate is worse when we include the effects of extinction. Our final Le PHARE output is therefore obtained using the eight Poggianti templates and neglecting the effects of extinction by dust in the host galaxy. We use the five-band *ugriz* photometry in the SDSS filters as this gives significantly more accurate photometric redshifts compared to the case when we remove the *u*-band photometry with the largest photometric errors.

3.1.6 ZEBRA – Zurich Extragalactic Bayesian Redshift Analyzer

The Zurich Extragalactic Bayesian Redshift Analyzer (Feldmann et al. 2006) is a more sophisticated Bayesian template-fitting photometric redshift code compared to its predecessor, BPZ. The basic principles of estimating redshifts using templates and Bayesian priors remain as described in Section 3.1.4 but among the novel techniques employed within the ZEBRA package are the photometry check mode that checks and corrects the photometry in certain filters, a template optimization mode to improve the standard set of templates in specified redshift bins using a training set of galaxies

with spectroscopic redshifts, and the ability to calculate a prior self-consistently from the photometric catalogue when ZEBRA is run in its Bayesian mode.

We choose not to employ the photometry check mode within ZEBRA as we are fairly confident that we have reliable photometry for our objects and have checked that applying a catalogue correction does not improve the photometric redshifts.

ZEBRA's template set consists of the standard E, Sbc, Scd and Im galaxies as well as the SEDs of the two starbursting galaxies SB2 and SB3. These are further interpolated in logarithmic space by ZEBRA during the photo-z estimation. We find that including the E, Sbc and Scd templates produces better results than including all the six templates. Furthermore, we use ZEBRA's template optimization mode to construct improved templates from these three basis templates in two redshift bins: $0 < z < 0.5$ and $0.5 < z < 1.0$. We use a regularization parameter of $\rho = 0.05$ and a plianliness parameter of $\sigma = 2$. Feldmann et al. (2006) gives details of these parameters and how to optimize them so as to produce the most realistic templates. We do not model intergalactic medium absorption in our templates as we find that this produces better photometric redshifts. The optimization procedure produces 39 basis templates and we use these along with our original templates in the photometric redshift calculation.

We find the Bayesian mode of ZEBRA to produce considerably better photometric redshifts than the maximum likelihood mode and we therefore consider only outputs from the Bayesian mode when calculating figures of merit. The Bayesian mode is run using four iterations to calculate the prior self-consistently from the photometric catalogue. Further iterations slightly worsen the photo-z estimate. We use a smoothing kernel to smooth the prior after every iteration.

4 RESULTS

Here we summarize the results obtained when running our different public photo-z codes on the 2SLAQ sample of 5482 LRGs. Note that each of the photo-z codes detailed in Section 3.1 has been run several times using different parameters in order to optimize them to produce the best photo-z estimate. The final output files from each code used in this analysis are ones that gave the best photo-z estimate. Hence this is not only a code comparison but also a code plus library comparison which is the final publicly available product to the non-expert online. The configuration files used to calculate the final photo-z estimates for each of the codes are provided online along with the full catalogue.³

We note here that this is not a comparison that is meant to contrast equal values. For instance it is already well accepted that training codes work much better within the redshift and spectral energy distribution range present in the training set but template methods are superior if there are objects in the survey outside this range. Template methods also provide accurate error estimates as well as other physical parameters for the galaxy whereas ANNz provides an error estimate based on the photometric errors and can be adjusted to provide physical parameters but only if they are known for the training set (Abdalla et al. 2008; Banerji et al. 2008). Also, codes such as BPZ provide an automatic selection of the objects with the best photo-z estimates via for example the odds parameter. The purpose here is to compare the

² <http://www.oamp.fr/people/arnouts/LE PHARE.html>

³ www.ast.cam.ac.uk/~mbanerji/Research/MegaZLRGDR6/megaz.html

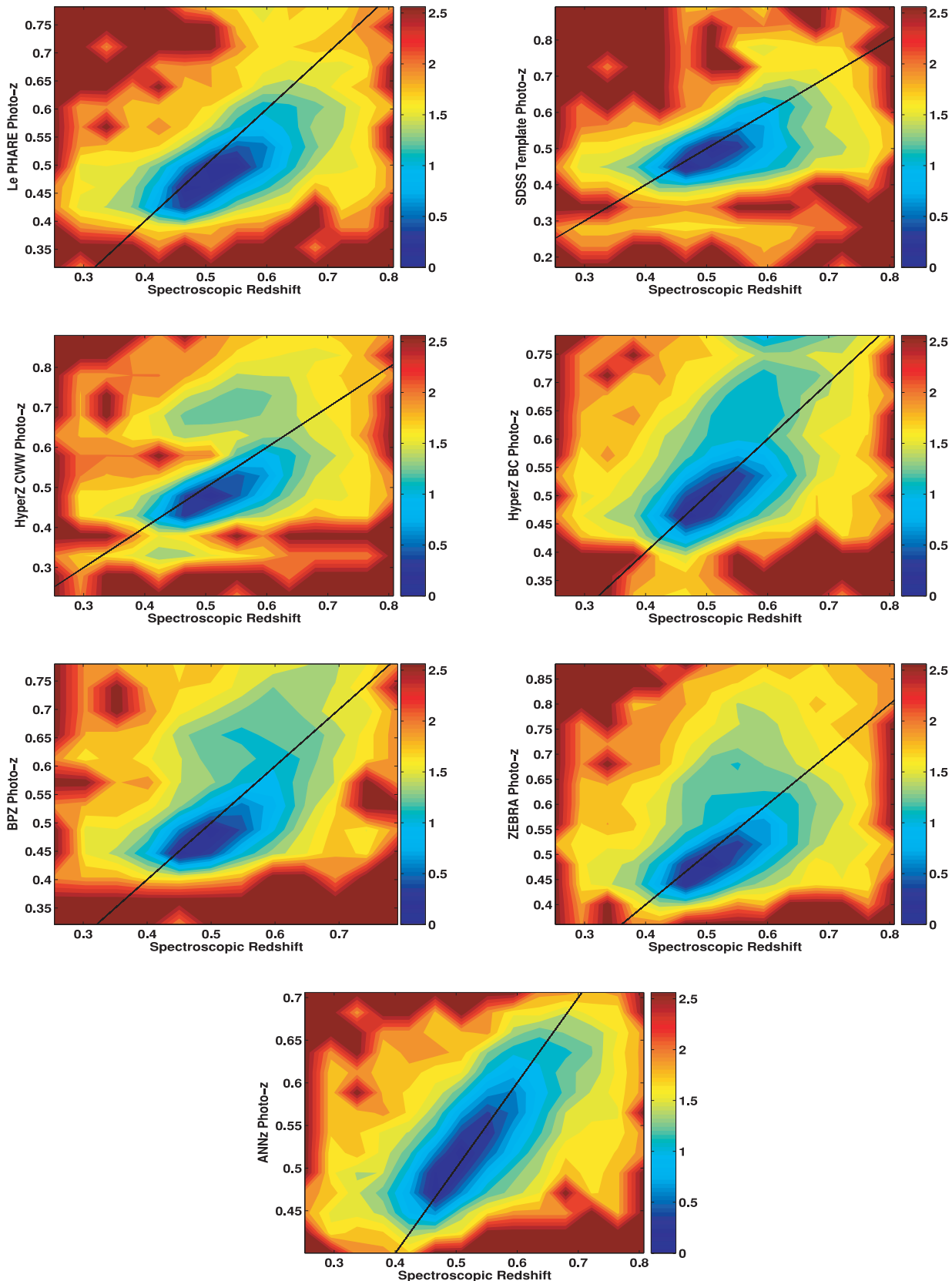


Figure 2. Density plots of spectroscopic versus photometric redshift for each of the public photo- z codes described in Section 3.1. The plots are colour-coded and the scale is exponential. A colour difference of 1 is equivalent to the density being decreased by a factor of e . The solid black lines show where the spectroscopic redshift is equal to the photometric redshift.

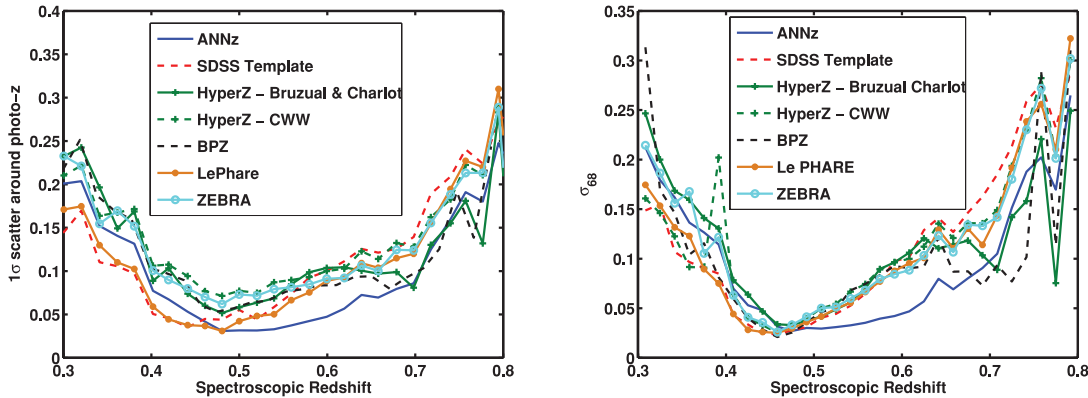


Figure 3. The 1σ scatter on the photometric redshift around the true spectroscopic redshift, defined as per equation (6) for each of the public photo- z codes described in Section 3.1, is in the left-hand panel and σ_{68} as a function of the spectroscopic redshift for each of the public photo- z codes described in Section 3.1 is in the right-hand panel.

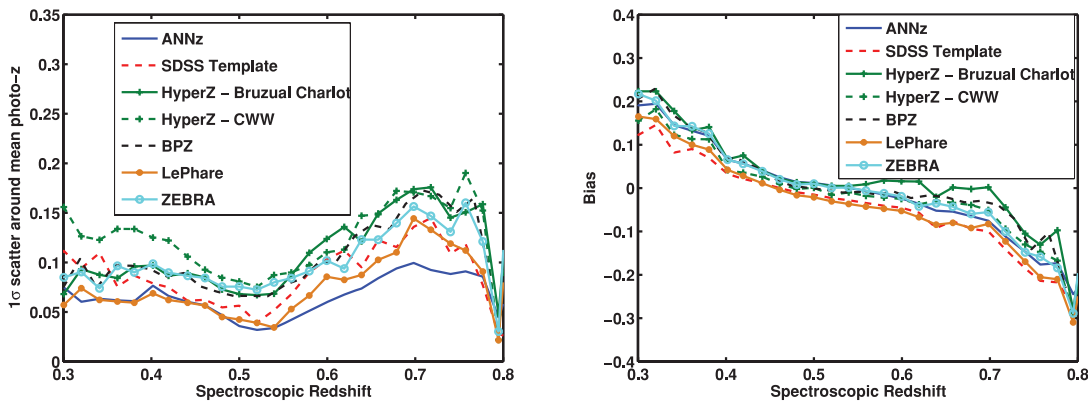


Figure 4. The 1σ scatter around the mean photometric redshift plotted as a function of spectroscopic redshift according to equation (8) (left-hand panel) and bias as a function of spectroscopic redshift (right-hand panel). We can see that there is a similar trend for most codes but a difference is present. In these metrics it seems that the training code is better suited to the scatter but not for the bias. We can see from the next two figures that the opposite is true.

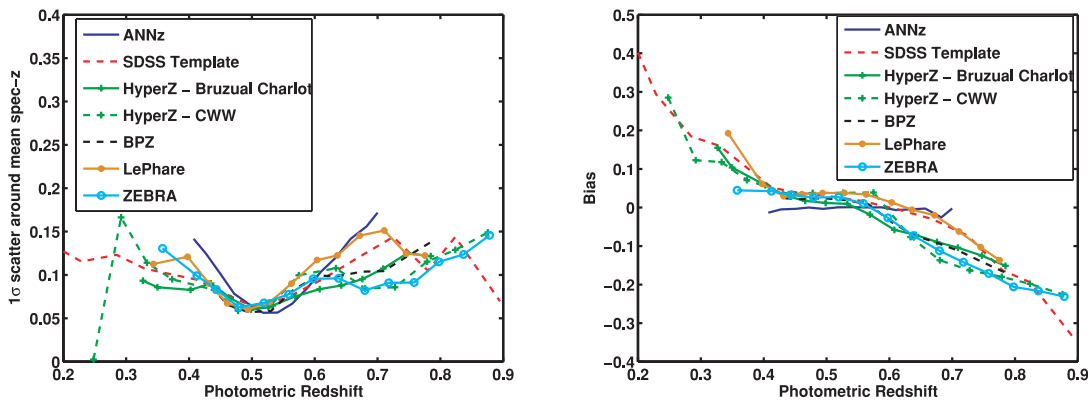


Figure 5. The 1σ scatter around mean spectroscopic redshift as a function of photometric redshift according to equation (9) is in the left-hand panel and the bias as a function of photometric redshift is in the right-hand panel. We can clearly see the power of the training code looking at the bias graph; ANNz performs with virtually no bias. However, this has a certain drawback, the scatter around the mean spectroscopic redshift is larger in certain areas as a function of photometric redshift. Clearly, different methods produce results of different quality depending on the figure of merit used. We note, e.g. that ANNz has a limited coverage in photo- z as the training set is confined to that redshift range.

full packages, including SEDs and features available from different codes. Furthermore, the chosen sample of LRGs has a very narrow range of SEDs and this comparison therefore does not highlight the strength of photometric redshift codes with a broad

range of library templates that would be more suitable for other samples.

In Fig. 2 we plot density plots of the spectroscopic redshift versus photometric redshift for each of these different codes.

In order to evaluate the precision with which each of these different codes calculates the photometric redshift, we can look at the 1σ scatter between the true (spectroscopic) redshift and the photometric redshift. This is defined as follows:

$$\sigma_z = \langle (z_{\text{phot}} - z_{\text{spec}})^2 \rangle^{1/2}. \quad (6)$$

This quantity is plotted in the left-hand panel of Fig. 3. As expected, the empirical photo- z estimator ANNz seems to work best at intermediate redshifts where there are a large number of representative training set galaxies. At high redshifts, HyperZ BC provides us with the best estimates of the photometric redshift. At low redshifts, the SDSS code and Le PHARE template-fitting codes perform the best. We note that none of these runs used the more standard CWW templates, suggesting that these templates are not a good match to the LRGs that are being analysed in this study.

As can be seen in Fig. 2, however, there are many outliers present in our sample. Another useful quantity to consider is therefore σ_{68} which is the interval in which 68 per cent of the galaxies have the smallest difference between their spectroscopic and photometric redshifts. We note that σ_{68} and σ_z are equal only if the distribution of redshifts is Gaussian. This will give us some indication of the scatter in the photometric redshift estimate once the outliers have been removed; it is plotted in the right-hand panel of Fig. 3.

Another important quantity used to quantify how good a photo- z estimate is, is the bias defined as

$$b_z = \langle z_{\text{phot}} - z_{\text{spec}} \rangle. \quad (7)$$

This quantity is plotted for each of the different codes, in the right-hand panel of Fig. 4. Padmanabhan et al. (2005) show that galaxies with a given photometric redshift often have a systematic bias on them and this bias can therefore be added to those photo- z galaxies in order to correct for it. In order to get an idea about the error on the photometric redshift once this bias has been corrected for, we plot in the left-hand panel of Fig. 4 the 1σ scatter around the mean photometric redshift estimate in each bin, defined as follows:

$$\sigma_{z2} = \langle (z_{\text{phot}} - \bar{z}_{\text{phot}})^2 \rangle^{1/2}. \quad (8)$$

As can be seen, the scatter is now reduced for most of the codes as we are not accounting for any systematic shift that can be corrected. The bias is largest at high redshifts for the SDSS and Le PHARE template-fitting codes and these codes have the biggest improvement in the scatter at high redshifts when we take the moment around the mean rather than the true redshift.

A more useful measure for future surveys is to plot the bias and scatter as a function of the photometric redshift as in Fig. 5. The 1σ scatter around the mean spectroscopic redshift estimate in each photo- z bin is defined as follows:

$$\sigma_{z3} = \langle (z_{\text{spec}} - \bar{z}_{\text{spec}})^2 \rangle^{1/2}. \quad (9)$$

We can also compare the right-hand panels of Figs 4 and 5 to each other. We can see that the bias follows the same trend as a function of spectroscopic redshift for all the different photo- z codes and is fairly similar for all these codes. However, the bias as a function of the photometric redshift is very different for the different photo- z codes and a better indicator of how much the photo- z estimate has to be corrected for systematic errors. This bias is almost flat for the training method which has enough training set galaxies to effectively minimize the bias through the training process. The integral under the curve is also small for ZEBRA as shown in Table 2 as the template optimization technique here

Table 2. Average 1σ scatter (equation 6) and bias (equation 7) for the entire sample for different methods. This is yet another metric to use if the redshift dependence of the bias and scatter is not of interest. Note that the definition of the 1σ scatter here is different from that in Collister et al. (2007), equation (10).

Method	σ_z	Bias
ANNz	0.0575	0.0014
SDSS	0.0808	-0.0264
HyperZ CWW	0.0973	-0.0076
HyperZ BC	0.0862	0.0160
LePHARE	0.0718	-0.0302
ZEBRA	0.0898	0.0013
BPZ	0.0933	0.0112

Table 3. Fraction statistics for the different codes presented in this section. The fractions f_0 – f_4 are defined in the following way. The galaxies are divided into a matrix defined along the axes in the photo- z /spec- z plane. The fraction f_0 is the fraction of galaxies which is on the diagonal of this matrix. The fraction f_1 is the fraction of galaxies in the first off diagonals of the matrix and so on. The grid is defined with the following boundaries in redshift $z = [0.2, 0.4, 0.5, 0.6, 0.7, 0.9]$. We can see from the table that different methods provide different number of outliers. Given the nature of the galaxies the outlier fraction is small in each method but still is relatively different across methods.

Method	f_0 (per cent)	f_1 (per cent)	f_2 (per cent)	f_3 (per cent)	f_4 (per cent)
ANNz	37	28	31	4	0.02
SDSS	27	31	37	4.5	0.8
HyperZ CWW	24	32	35	7	1.5
HyperZ BC	26	32	32	7	1.5
LePHARE	26	34	34	4	0.5
ZEBRA	26	34	34	5	0.8
BPZ	24	32	36	6	1

was able to remove the average bias for the entire redshift range. However, a remaining bias was found at high and low redshifts with the values of the ZEBRA configuration parameters used in this analysis.⁴

We also present in Table 2 the integrated bias and scatter for all the codes and libraries we have used. We can see that the training code performs best which is to be expected with a complete training set and that the bias here is very small. However, this statistic does not show the redshift dependence of the scatter or bias which may be of interest depending on the application.

As an alternative statistic, we present in Table 3 the fraction statistics for the methods presented in this section. The fractions f_i are defined as the fraction of galaxies in certain regions of the photo- z /spec- z plane. If we divide this plane into rectangular regions, the fraction f_0 is the fraction of galaxies which is on the diagonal of this matrix. We could have subdivided the areas along the diagonals, this would have been a suitable statistic as well. However, there are

⁴ It is possible that a better choice of template optimization parameters could be found resulting in the removal of the bias at low and high redshifts. However, since the intent of this paper is to perform a code comparison from the point of view of the photo- z user rather than the photo- z developer, and since it is not obvious what this better choice of parameters would be, we choose to leave our results as they are.

reasons for which the statistic we quote is interesting. For instance if one is interested in cosmological probes where the galaxies are separated in photo- z bins, then a subdivision along the photo- z axis is more natural. Given that these galaxies are relatively red with good photometric redshifts, we can see that the fraction of outliers is small for all estimators. However, there is still a difference between different implementations of publicly available codes.

5 SYSTEMATIC CHECKS ON THE PHOTOMETRIC CATALOGUES

The clustering of the SDSS LRG photometric sample has been analysed using the SDSS code for photometric redshifts described in section 3.1.1 of Padmanabhan et al. (2007) and by ANNz described in section 3.1.3 of Blake et al. (2007). For the rest of this section

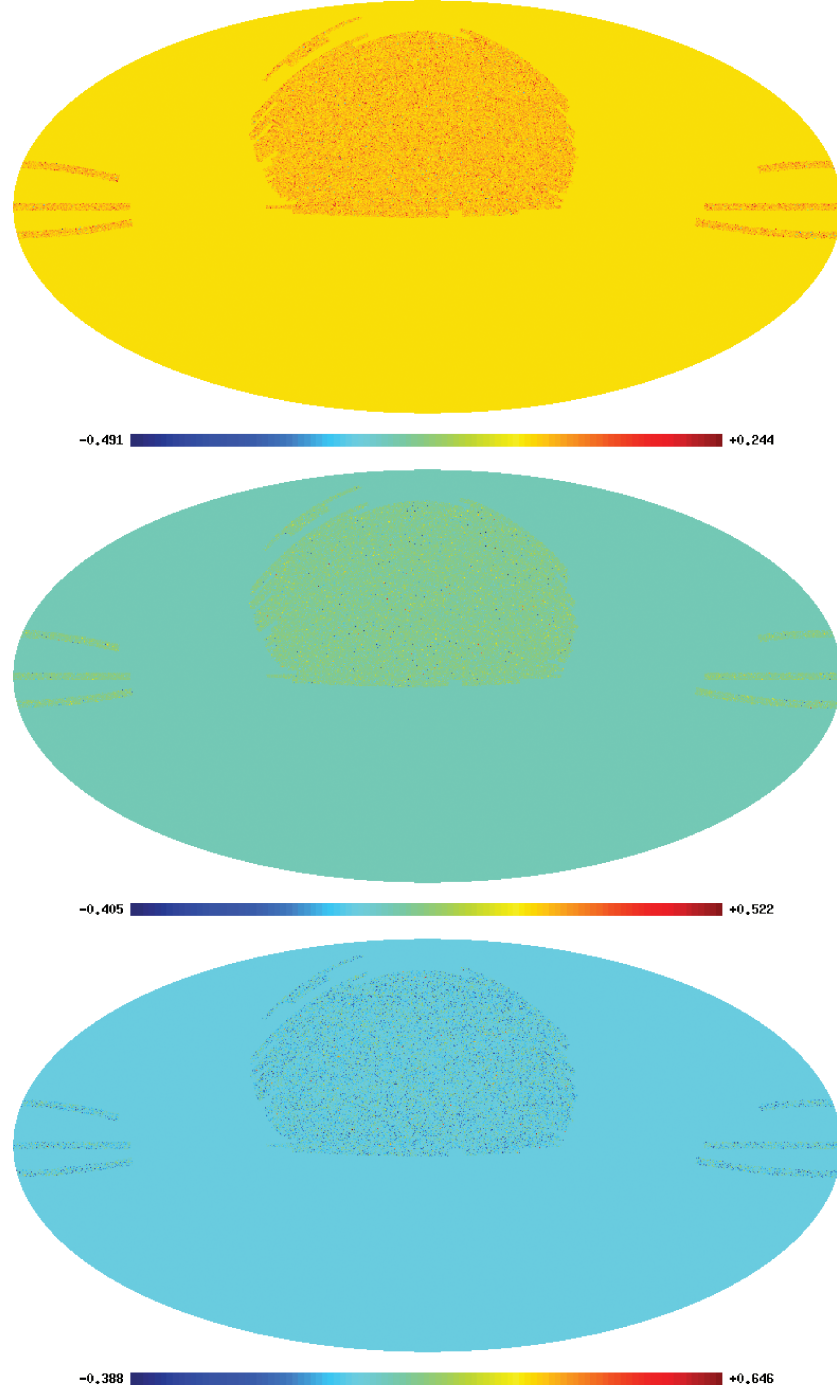


Figure 6. (Best seen in colour) The bias between the photo- z estimate from ANNz and the photo- z estimate from SDSS. This has been subdivided into bins according to the photo- z estimate from ANNz. The redshift bins are 0.4–0.5 (top), 0.5–0.6 (middle) and 0.6–0.7 (bottom). We can clearly see from the colour coding that there is a bias as a function of redshift. If the bias is disregarded and we look at the variation across the sky, there is no evidence that there is a gradient or that the photometric redshifts are different closer to the regions from which the training set was drawn. The random nature of the residual bias shows that the extrapolation in sky position and calibrations are done to a sufficient accuracy and that the photo- z estimates are statistically reliable in the plane of the sky.

we choose to look more in detail at the effects that these two codes have on the end products of the analysis. We check for gradients in the photo-z distribution across the sky. These gradients should be present if the training set for the neural networks is biased as a function of position in the sky.

5.1 Checking for gradients in redshift difference across the sky

It is difficult to trust two very different techniques such as template-fitting methods and training methods to produce consistent results without making a comprehensive comparison of both methods on the same set of galaxies. Given that the training set from the training method is drawn from a small region of the sky with a limited range of galactic extinction, one could assume a priori that this extra calibration which is necessary might introduce biases as a function of sky position in applications of empirical methods. This would be dramatic in the case of, for instance cosmological studies where we are attempting to calculate variations across the sky to infer cosmological parameters.

We have looked for gradients in the difference $dz = z_{\text{ANNz}} - z_{\text{SDSS}}$ in three redshift shells, $0.4 < z_{\text{phot}} < 0.5$, $0.5 < z_{\text{phot}} < 0.6$ and $0.6 < z_{\text{phot}} < 0.7$. We have separated galaxies in each redshift bin according to the ANNz photometric redshift. If the separation were done with the SDSS photometric redshifts instead, the result would not have changed a lot. The values of dz were taken as an average value in pixels produced with HEALPIX, hence are smoothed to produce the maps in Fig. 6. No apparent gradients can be identified, in any of the redshift shells, which is an indicator for the consistency across the plane of the sky.

The different colour coding in each of the redshift shells in Fig. 6 is indicative of the bias between the two methods which is of course still present; however, taking that bias aside, there seems to be no correlation between the usual regions of high extinction in the SDSS regions and the scatter of biases as a function of sky position produced here. Given that the template set does not know about the training set which belongs to a selective region of the sky, our conclusion is that the fact that the training set is restricted to a small region of the sky does not include significant biases as a function of sky position and therefore is not an extra source of systematic biases. This could be taken further, for instance by calculating spherical harmonics of the map above and comparing with theoretical predictions in order to estimate the actual lower bound of a potential systematic effect for a given probe but since this would involve a more specific cosmological approach we argue that this is beyond the photometric redshift comparison which is the aim of this paper.

The main reason why there could be a systematic bias as a function of sky position is extinction. We have computed the difference between the two photo-z estimates for different regions of galactic extinction and plotted histograms for these quantities in Fig. 7. Apart from the normalization which encoded the fact that there are different numbers of galaxies in these bins, the curves agree in bias and scatter; this also shows that there is no evidence for a variation in the bias as a function of extinction. This can only get better with future *Planck* data as it will measure the dust extinction within our galaxy with a resolution of around 10 arcmin. So we are confident that this is not a systematic effect that will hinder future or current photometric redshift analyses.

5.2 A photo-z comparison of the codes

We also present here a comparison of how the photometric redshifts of each code compare to those of the other codes. We present in

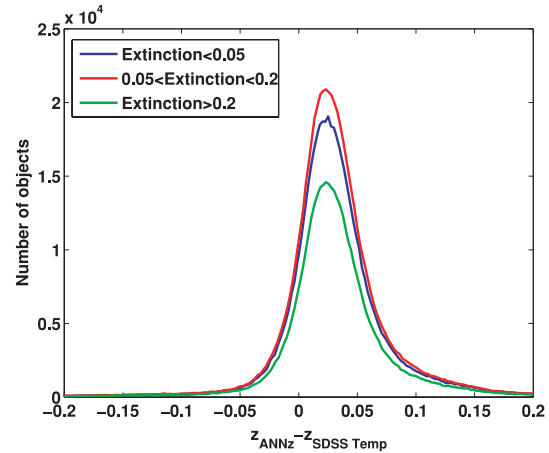


Figure 7. Histograms of the difference between the photometric redshifts from the ANNz code and from the SDSS template-fitting code. We can see that the curves are identical apart from the normalization which is due to the different number of galaxies in each bin. This shows that the Milky Way extinction is not producing a significant bias in the photometric redshifts given that one has a training set which is limited in the area in the sky.

Fig. 8 histograms of the difference between photo-z for each pair of codes that we have used in the analysis of our updated MegaZ-LRG catalogue. We can see that the differences between codes is apparent in some plots.

For instance, when comparing ANNz to other codes there seem to be some outliers at a redshift difference of 0.1 compared to HyperZ CWW, BPZ and HyperZ BC. Similarly, other pairs of codes produce outliers which indicates that this is not only a difference between template codes and training codes. We also note that for instance comparing ZEBRA with codes such as HyperZ CWW or SDSS code, there is a good agreement on the scatter but there is a small bias between the codes which may suggest that the templates used might not have been optimal in some codes. We note that there are techniques to remove the bias by calibrating the templates (Ilbert et al. 2006) using a training set. The IMPZ code (Rowan-Robinson, private communication) was also tested on the sample of 5482 2SLAQ LRGs and it has produced results consistent with other template-based methods. However, as the code in its current form is not yet publicly available, we do not present these results here or extend the analysis to the MegaZ-LRG DR6 catalogue described in the next section.

We emphasize here that there are many differences even though all the photo-z estimates are of relatively good quality. There is therefore a need to deconstruct the effects of the algorithm and the template libraries in order for us to understand these differences and have even more reliable photo-z estimates in the future.

6 AN EXTENSION TO MEGAZ-LRG: CATALOGUES WITH DIFFERENT PHOTO-Z ESTIMATORS FOR SDSS DR-6

We have extended the photometric sample from SDSS DR4 to SDSS DR6 imaging catalogue using the same criteria devised for the 2SLAQ LRG catalogue. This extended MegaZ-LRG catalogue contains 1543 596 objects over more than 8000 deg² of the

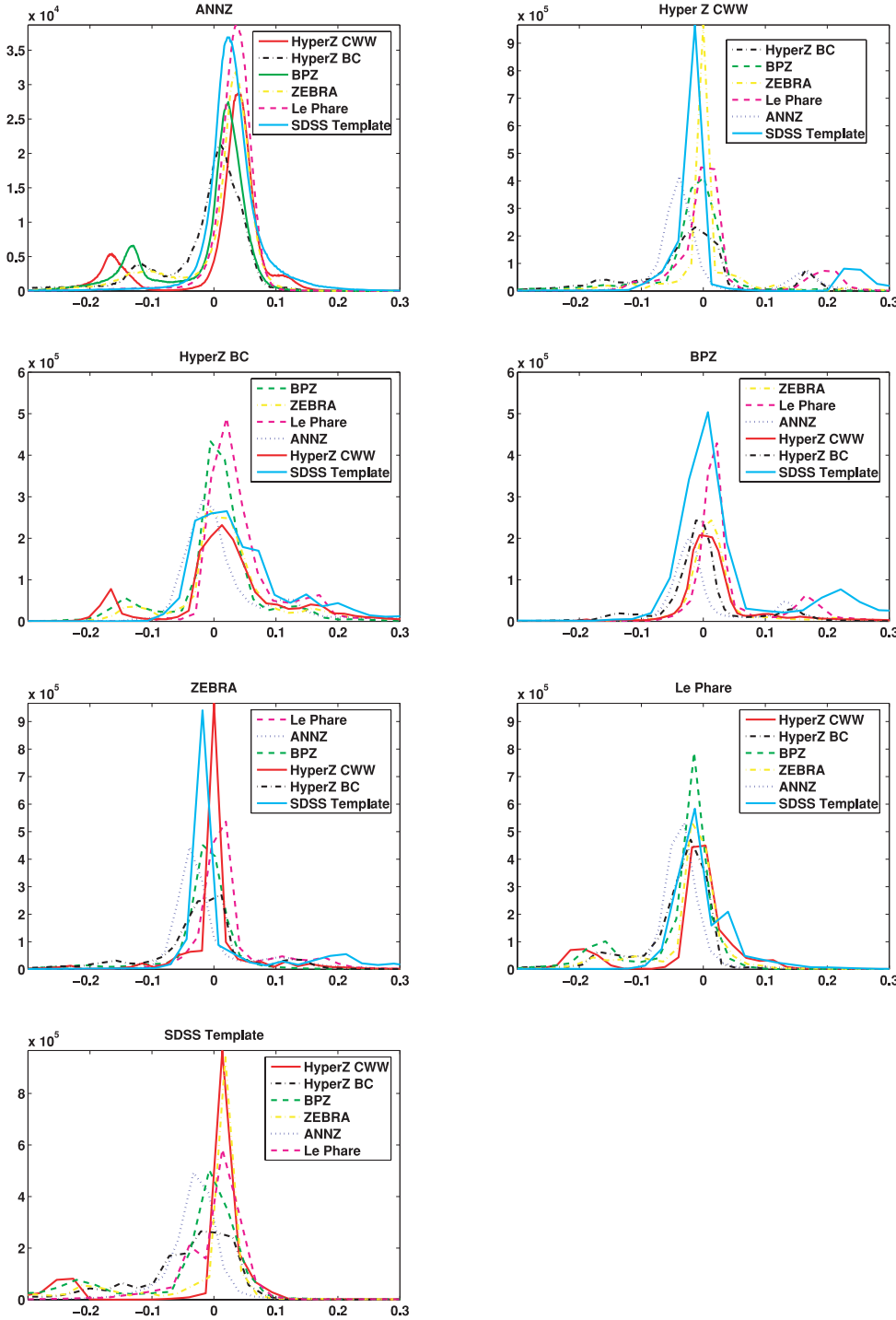


Figure 8. Histogram of the difference between the photometric redshift estimation for all the pairs of codes we have used in this analysis.

sky. As for previous studies, LRGs are expected to be about 95 per cent of the sample and M-type stars are expected to be 5 per cent of the sample. We have produced photometric redshift results for seven different photometric redshift estimators and provided the error estimators associated with each method. We also provide trained empirical values to perform star/galaxy separation based on a set of 15 photometric parameters as in Collister et al. (2007). All

the parameters included in the revised catalogue are described in Table 4. The data can be found in the web site of which the URL is given in the footnote⁵ along with configuration files for all the codes presented in this work.

⁵ www.ast.cam.ac.uk/~mbanerji/Research/MegaZLRGDR6/megaz.html

Table 4. Parameters included in the updated MegaZ-LRG DR6 photometric redshift catalogue.

objID	SDSS objID
ra	J2000 right ascension
dec	J2000 declination
dered_u	
dered_g	
dered_r	Dereddened model magnitudes
dered_i	
dered_z	
err_u	
err_g	
err_r	Magnitude errors
err_i	
err_z	
deVMag_i	Dereddened de Vaucouleurs magnitude
z_an nz	ANNz photometric redshift
z_an nz_err	ANNz photometric redshift error
delta_sg	ANNz galaxy probability
delta_err_sg	ANNz galaxy probability error
z_sdss	SDSS photometric redshift
z_hz cww	HyperZ CWW photometric redshift
z_hz cww_chi	HyperZ CWW chi-squared
z_hz cww_errl	HyperZ CWW photometric redshift 68 per cent lower confidence limit
z_hz cww_errh	HyperZ CWW photometric redshift 68 per cent higher confidence limit
z_hzbc	HyperZ BC photometric redshift
z_hzbc_chi	HyperZ BC chi-squared
z_hzbc_errl	HyperZ BC photometric redshift 68 per cent lower confidence limit
z_hzbc_errh	HyperZ BC photometric redshift 68 per cent higher confidence limit
z_bpz_bayes	BPz Bayesian photometric redshift
z_bpz_errl	BPz photometric redshift 90 per cent lower confidence limit
z_bpz_errh	BPz photometric redshift 90 per cent higher confidence limit
z_bpz_odds	BPz Bayesian odds parameter
z_bpz_ml	BPz maximum likelihood photometric redshift
z_bpz_chi	BPz chi-squared
z_zebra	ZEBRA photometric redshift
z_zebra_errl	ZEBRA photometric redshift 68 per cent lower confidence limit
z_zebra_errh	ZEBRA photometric redshift 68 per cent higher confidence limit
z_lp	Le PHARE photometric redshift
z_lp_prob	Le PHARE percentage PDF between $dz = z_{\text{best}} \pm 0.1(1 + z_{\text{best}})$

7 CONCLUSIONS

We have presented an updated version of the MegaZ-LRG catalogue. This catalogue contains about 1.5 million objects with accurate photometric redshifts which can be used for a range of science applications. The catalogue is available online and contains SDSS ID information, so all the SDSS data can be retrieved for each object as well as the photometric redshifts from each of the six public codes.

We have run several comparisons of code and template libraries on the 2SLAQ LRG sample. Our experience was that some codes were particularly user friendly, for instance we believe that HyperZ is still very popular given its ease of use. Other codes are harder to tweak given the use of HyperZ parameters, such as the ZEBRA code. Computationally, most template-fitting codes benchmark roughly similarly as opposed to training codes which are much faster to evaluate the redshifts but only once training is complete. We conclude that there are differences among the codes and stress that a more thorough comparison is needed where the effects of the codes and template libraries are disentangled. This will allow us to pinpoint where the discrepancies are arising. An approach based on first principles such as that presented in Budavári (2009) is also

timely. We have used several figures of merit to assess which code + template library performed best for this set of galaxies. We conclude that different codes perform with different strengths depending on the figure of merit used. We outline the findings more specifically below.

- (i) As expected, the availability of a complete training set means the training method, ANNz, performs best in the intermediate redshift bins where there are plenty of spectroscopic redshifts.
- (ii) Le PHARE performs very well particularly in the lower redshift bins, suggesting that the Poggianti templates may be a better fit to LRGs at those redshifts compared to other templates used in this comparison.
- (iii) HyperZ run with Bruzual & Charlot templates gives better results than using the same with CWW templates, once again highlighting the importance of template choice.
- (iv) The SDSS template code gives very good results compared to other codes at the highest photo-z bins despite having only one evolving template for the LRGs. Given the narrow range in the SEDs of our sample of LRGs, the strengths of template-based codes with extensive template libraries are not adequately highlighted by this comparison.

(v) ZEBRA shows a small average bias, indicating the importance of the template optimization technique in removing biases. The main sources of differences among the template codes are the differences in the templates, hence one should emphasize the template corrections in their photo-z analysis.

As expected, the training code performs best where the training set is large and complete and the template sets overtake the training code if the training set starts to become sparse. The importance of template choice is highlighted by the fact that most figures of merit show codes used in conjunction with the CWW templates to perform worse than those using other training or synthetic templates. This suggests that the CWW templates are not a very good match to the SEDs of these LRGs.

There is a discrepancy between the scatters found for these codes, ranging from 0.057 to 0.097. Both the values are considered as good results for photo-z estimates as one would expect from LRGs but there is a clear difference between the different code and template combinations that have been run. Given that these differences will also depend on galaxy type and training set size, it is imperative that we carry out a more thorough comparison where the effects of codes and templates are deconstructed, in order to understand what factors affect the photo-z accuracy. We caution the reader that the results presented here are specific to a subsample of galaxies, namely LRGs, which have a narrow range in SEDs, and that a complete and representative spectroscopic training set is available. The conclusions presented here could, and probably would, change if the comparisons were made with different galaxies or a different training set size.

We have also produced a set of tests to assess whether the fact that the training sets are from a restricted area in the sky affects the photometric redshifts significantly. We conclude that there is little or no difference between the results from template methods and training set methods across the sky and that the difference found is not likely to be a reason for the training set being restricted in area. This is promising for future wide-field photometric redshift surveys such as the Dark Energy Survey, PanStarrs, *Euclid* and *JDEM*.

ACKNOWLEDGMENTS

We thank Stephane Arnouts, Tom Babbedge, Narciso Benitez, Michel Bolzonella, Marcella Carollo, Nikhil Padmanabhan and Michael Rowan-Robinson for useful comments regarding the publicly available codes and also for checking that our usage of the codes was acceptable. FBA acknowledges the support of a Leverhulme Early Careers Fellowship and the Royal Society for an University Research Fellowship. MB is supported by an STFC studentship. OL would like to acknowledge the Royal Society Wolfson Research Merit Award.

REFERENCES

- Abdalla F. B., Rawlings S., 2005, MNRAS, 360, 27
 Abdalla F. B., Amara A., Capak P., Cypriano E. S., Lahav O., Rhodes J., 2008, MNRAS, 387, 969
 Arnouts S. et al., 2002, MNRAS, 329, 355
 Assef R. J. et al., 2008, ApJ, 676, 286
 Babbedge T. S. R. et al., 2004, MNRAS, 353, 654
 Banerji M., Abdalla F. B., Lahav O., Lin H., 2008, MNRAS, 386, 1219
 Benítez N., 2000, ApJ, 536, 571
 Blake C. A., Abdalla F. B., Bridle S. L., Rawlings S., 2004, New Astron. Rev., 48, 1063
 Blake C., Collister A., Bridle S., Lahav O., 2007, MNRAS, 374, 1527
 Blake C., Collister A., Lahav O., 2008, MNRAS, 385, 1257
 Blanton M. R., Roweis S., 2007, AJ, 133, 734
 Bolzonella M., Miralles J.-M., Pelló R., 2000, A&A, 363, 476
 Brammer G. B., van Dokkum P. G., Coppi P., 2008, ApJ, 686, 1503
 Bruzual G., Charlot S., 2003, MNRAS, 344, 1000
 Budavári T., 2009, ApJ, 695, 747
 Budavári T., Szalay A. S., Csabai I., Connolly A. J., Tsvetanov Z., 2001, AJ, 121, 3266
 Calzetti D., Kinney A. L., Storchi-Bergmann T., 1994, ApJ, 429, 582
 Cannon R. et al., 2006, MNRAS, 372, 425
 Cole S. et al., 2005, MNRAS, 362, 505
 Coleman G. D., Wu C.-C., Weedman D. W., 1980, ApJS, 43, 393
 Collister A. A., Lahav O., 2004, PASP, 116, 345
 Collister A. et al., 2007, MNRAS, 375, 68
 Connolly A. J., Csabai I., Szalay A. S., Koo D. C., Kron R. G., Munn J. A., 1995, AJ, 110, 2655
 Csabai I. et al., 2003, AJ, 125, 580
 Dalton G. et al., 2006, in McLean I. S., ed., Proc. SPIE 6269, Ground-based and Airborne Instrumentation for Astronomy. SPIE, Bellingham, WA, p. 62694A
 Feldmann R. et al., 2006, MNRAS, 372, 565
 Fioc M., Rocca-Volmerange B., 1997, A&A, 326, 950
 Firth A. E., Lahav O., Somerville R. S., 2003, MNRAS, 339, 1195
 Hildebrandt H., Wolf C., Benítez N., 2008, A&A, 480, 703
 Ilbert O. et al., 2006, A&A, 457, 841
 Kinney A. L., Calzetti D., Bohlin R. C., McQuade K., Storchi-Bergmann T., Schmitt H. R., 1996, ApJ, 467, 38
 Komatsu E. et al., 2009, ApJS, 180, 330
 Koo D. C., 1999, in Weymann R., Storrie-Lombardi L., Sawicki M., Brunner R., eds, ASP Conf. Ser. Vol. 191, Photometric Redshifts and the Detection of High Redshift Galaxies. Astron. Soc. Pac., San Francisco, p. 3
 Lahav O., Abdalla F. B., Banerji M., 2008, in Hobson M., Liddle A., Mukherjee P., Parkinson D., eds, Bayesian Methods in Cosmology. Cambridge Univ. Press, Cambridge
 Loh E. D., Spillar E. J., 1986, ApJ, 303, 154
 Madau P., 1995, ApJ, 441, 18
 Padmanabhan N. et al., 2005, MNRAS, 359, 237
 Padmanabhan N. et al., 2007, MNRAS, 378, 852
 Percival N. et al., 2007, ApJ, 657, 645
 Rowan-Robinson M. et al., 2008, MNRAS, 386, 697
 Thomas S. A., Abdalla F. B., Lahav O., 2010, Phys. Rev. Lett., 105, 1301
 Thomas S. A., Abdalla F. B., Lahav O., 2011a, MNRAS, 412, 1669
 Thomas S. A., Abdalla F. B., Lahav O., 2011b, Phys. Rev. Lett., 106, 1301
 Wolf C. et al., 2001, A&A, 365, 681

This paper has been typeset from a \TeX / \LaTeX file prepared by the author.